Regular Article

PHYSICAL CHEMISTRY RESEARCH
Published by the
Iranian Chemical Society
www.physchemres.org
info@physchemres.org

Phys. Chem. Res., *Vol. 5, No. 2, 253-268, June 2017*
DOI: 10.22036/pcr.2017.40858

Sono-synthesis of Novel Magnetic Nanocomposite (Ba-α-Bi_2O_3-γ-Fe_2O_3) for the Solar Mineralization of Amoxicillin in an Aqueous Solution

S. Ramandi[a], M.H. Entezari[a,b,*] and N. Ghows[a]

[a]*Sonochemical Research Center, Department of Chemistry, Ferdowsi University of Mashhad, 91779, Mashhad, Iran*
[b]*Environmental Chemistry Research Center, Department of Chemistry, Ferdowsi University of Mashhad, 91779, Mashhad, Iran*
(Received 29 September 2016, Accepted 29 November 2016)

In this study, a novel magnetic nanocomposite (Ba-α-Bi_2O_3-γ-Fe_2O_3) was successfully synthesized through a combination of ultrasound and co-precipitation method under mild conditions. The structure of the synthesized nano-composite as a visible light photocatalyst was investigated by the X-ray diffraction (XRD), transmission electron microscopy (TEM), high resolution transmission electron microscopy (HRTEM), Fourier transform infrared spectroscopy (FTIR), ultraviolet-visible spectroscopy (UV-Vis), energy dispersive X-ray spectroscopy (EDX), vibrating sample magnetometer (VSM) and photoluminescence (PL). The HRTEM confirmed that the nano-magnetic composites are rods with diameters of 10-12 nm and lengths of 100-200 nm. The photocatalytic activities of Ba-α-Bi_2O_3-γ-Fe_2O_3, α-Bi_2O_3-γ-Fe_2O_3, α-Bi_2O_3 and γ-Fe_2O_3 were compared by the degradation efficiency of amoxicillin as an antibiotic drug under solar light. On the basis of the results, amoxicillin in aqueous solution was more efficiently photodegraded using Ba-α-Bi_2O_3-γ-Fe_2O_3 as nanocomposite under solar light irradiation. The degradation reached to 99% and the mineralization reached to 55% within 2 h under sunlight. In addition, the results of degradation were fitted to the first-order kinetics model and the kinetic constant was 0.017 min^{-1} with a half-life time of 40 min. On the basis of the performed experiments, the photogenerated electrons played an important role in the decomposition process. In addition, it was confirmed that the formation of oxidative species such as singlet oxygen and superoxide radical in the presence of oxygen are the major factors in the destruction.

Keyword: Nanocomposite, Ultrasound, Solar light, Amoxicillin, Decomposition

INTRODUCTION

Recently, semiconductor photocatalysts have been actively studied for the treatment of wastewater [1-6]. This is due to their high potential in the degradation and mineralization of the harmful organic pollutants with low negative effects [7]. In addition, the photocatalytic performance under ambient conditions [8] and reusing after some pre-treatments are the advantages of these kinds of catalysts. Among the various photocatalysts, TiO_2 and ZnO have been considered as efficient photocatalysts. They absorb UV light that greatly limits their practical applications [9-11]. On the other hand, visible light photocatalysts have received considerable attention because of using of a solar light. Some of the semiconductors are unstable under solar light illumination (*e.g.,* CdS, CdSe) [12] or have low activity (*e.g.*, Fe_2O_3) [13] due to the recombination of photogenerated holes (h^+) and electrons (e^-) which lowers the quantum yield and wastes energy. Therefore, finding novel routes to develop new and more effective visible-light photocatalysts is today an important scientific and technological challenge.

In particular, bismuth trioxide (α-Bi_2O_3) is considered as a good choice for application in the field of gas sensors, superconductors, solid-state electrolytes, electro-chromic materials, solid oxide fuel cells, oxygen sensors, catalyst, and photocatalyst. This is due to its high oxygen-ion conductivity arising from infinite oxygen vacancies in the

*Corresponding author. E-mail: entezari@um.ac.ir

crystal structure [14-18,1] and its narrow band gap of 2.8 eV [18]. It can be excited by visible light [19,1], due to its relatively small band gap and higher oxidation power of the valence hole, however high electrical resistivity and phase instability under low oxygen partial pressures limits its application. Hence, its photocatalytic activity should be further improved to meet the requirements of environmental protection [20]. Constructing a heterojunction interface or coupling between the semiconductors with suitable potential energies is a useful method to enhance the photocatalytic activity due to the charge separation of electron-hole pairs and reduction their recombination [21-23]. There are very few reports of the formation of Bi_2O_3 coupled with semiconductors containing efficient photocatalysts under visible light irradiation, such as $BiVO_4/\alpha\text{-}Bi_2O_3$ [24], $BiOCl/\alpha\text{-}Bi_2O_3$ [25], $SrTiO_3/\alpha\text{-}Bi_2O_3$ [26], $ZrTiO_4/\alpha\text{-}Bi_2O_3$ [27], $CeO_2/\alpha\text{-}Bi_2O_3$ [28], $NiO/\alpha\text{-}Bi_2O_3$ [29], $TiO_2/\alpha\text{-}Bi_2O_3$ [20], and $\alpha\text{-}Fe_2O_3/\gamma\text{-}Bi_2O_3$ [30].

Among photocatalysts, γ- Fe_2O_3 has been studied widely as a visible-light and magnetically separable photocatalyst due to its narrow band-gap (2.2 eV) and sensitive magnetic response [31,2]. However, it does not show an excellent photocatalytic activity because of rapid recombination of the light-generated charge carriers (electron-hole pairs) which cannot be efficiently transferred to the surface leading to a low efficiency [32-34,2]. Hence, it seems that the mentioned limitation can be eliminated materials such as Bi_2O_3 that is expected to make up the shortage of $\gamma\text{-}Bi_2O_3$ in utilizing visible-light. In addition, it has been found that substitution of elements such as Sr, Ca and Ba changes the structure and properties of Bi compositions through the creation of oxygen-site defects and lattice distortions. This is due to the charge and ionic size effects in substitution process which create oxygen vacancies and might be a key role in the photocatalytic properties [35-37].

Taking the advantages of the facts stated above, in this study, ultrasound was used for the synthesis of Ba doped nanocomposite to enhance the catalytic performance [38-40]. It was found that ultrasound is a facile and efficient process for the preparation of various nanostructures under milder conditions. Ultrasound improves the contact of the components in the nanocomposite, increases the crystallinity, and enhances the uniformity of the nanosized particles. These effects can be attributed to the high temperatures and pressures produced during the cavitation process [41,42,38,39].

The synthesized nanocomposite was applied for the degradation of amoxicillin (AMX) in solution. AMX is a pharmaceutical product belonging to the class of β-lactam antibiotics with high toxicity and its concentration in surface waters is in ranges from ng l^{-1} to μg l^{-1}. Its continuous input into the environment leads to chronic exposure of aquatic organisms which may pose risks [43, 44]. As AMX is resistant to bio-degradation processes, photocatalytic processes using semiconductors are the most appropriate tools for its degradation in comparison with other techniques such as biological degradation, activated carbon adsorption, air stripping and reverse osmosis [5,11, 45]. However, the photocatalytic decomposition of AMX by TiO_2 under UV light irradiation has been studied extensively [46]. It seems that finding a novel course to explore new visible-light photocatalysts for degradation of AMX is a great challenge.

It should be noted that no reports have been documented for the synthesis of $Ba\text{-}\alpha\text{-}Bi_2O_3\text{-}\gamma\text{-}Fe_2O_3$ nanocomposite by ultrasound and other methods. In addition, the degradation of amoxicillin in solution by the synthesized nanocomposite is completely new and novel.

EXPERIMENTAL

Materials

$FeCl_3.6H_2O$, Na_2SO_3, NH_3 (25%), HCl, NaOH, Bi $(NO_3)_3.5H_2O$, HNO_3 and $Ba(NO_3)_3$ were purchased from Merck and amoxicillin was provided from Sigma-Aldrich. These materials were used without further purification. Deionized water was also used for all experiments.

Procedure

Synthesis of $\gamma\text{-}Fe_2O_3$. The preparation of $\gamma\text{-}Fe_2O_3$ was carried out by ultrasonic bath irradiation (Branson, model 8510E-DTH, USA, 40 kHz, 250W) with some changes [47]. First, 6 ml of solution 2 M $FeCl_3.6H_2O$ (HCl 2 M used as a solvent) was added to 21 ml deionized water and then 4 ml of Na_2SO_3 (1 M) was added dropwise under ultrasonic irradiation (the color changed from red to yellow). The prepared solution was added to 160 ml ammonia (25%) under ultrasonic irradiation for 30 min and the black

precipitate was formed. The precipitate was washed with deionized water until its pH reached in less than 7.5. Then, 340 ml deionized water was added to it and the suspension was acidified with HCl (0.1 M) to pH about 3. The suspension was refluxed using aeration for 3 h at about 120 °C until its color changed from black to reddish-brown. The resulting product was washed by deionized water five times, dried at room temperature, and finally calcined at 400 °C for 30 min.

Synthesis of α-Bi_2O_3. The α-Bi_2O_3 nanoparticles were synthesized by ultrasonic irradiation. First, 0.97 g bismuth nitrate was dissolved in 10 ml of 1.12 M nitric acid. The prepared solution was added dropwise into 100 ml of 0.2 M NaOH aqueous solution under constant stirring (300 rpm). Then, sonication by 20 kHz apparatus was applied with an acoustic intensity of 14 W cm^{-2} at 10 °C for 75 min. After sonication, the white-green precipitate was centrifuged and washed by deionized water, three times, and ethanol, one time. The final product was dried in an oven for 2 h at 80 °C and then calcined at 300 °C for 30 min.

Synthesis of Ba-α-Bi_2O_3-γ-Fe_2O_3. The preparation of Ba-α-Bi_2O_3-γ-Fe_2O_3 nanocomposite was carried out as follows: First, 0.97 g bismuth nitrate dissolved in 10 ml of 1.12 M nitric acid. The obtained solution was added dropwise into 70 ml of 0.2 M NaOH aqueous solution while stirring at room temperature (solution A). Then, 0.03 g γ-Fe_2O_3 was dispersed in 30 ml of 0.2 M NaOH aqueous solution in a beaker by 20 kHz for 10 min (solution B). A and B solutions were mixed and sonicated by ultrasound (20 kHz) for 75 min at 10 °C. Then, barium nitrate (0.03 g) was added to the suspension under sonication. The color of the mixture was brown-orange during the sonication. Finally, the precipitate was centrifuged and washed by water, three times, and ethanol and then dried at 80 °C for 2 h and calcined at 300 °C for 30 min. In addition, a sample of α-Bi_2O_3-γ-Fe_2O_3 was prepared according to the above procedure without the addition of Ba $(NO_3)_3$.

Characterization of Nanoparticles

The morphology, structure, size, and optical properties of Ba-α-Bi_2O_3-γ-Fe_2O_3 nanocomposite were characterized by using XRD, TEM, high resolution HRTEM, UV-Vis spectroscopy, and FT-IR. The α-Bi_2O_3-γ-Fe_2O_3 sample was also investigated by using UV-Vis spectroscopy and FT-IR. The XRD patterns were examined by Bruker-axs, D8 Advance model at a scanning rate of 0.04°/sec, with CuKα radiation (λ = 1.5406 A°). The TEM and HRTEM of the samples were carried out by Philips CM30 300 kV from Netherlands. The optical characteristic of the prepared sample was measured by UV-Vis spectroscopy (Unico 2800 model). The FT-IR spectrum of the catalysts was investigated by Thermo Nicolet FT-IR (Avatar 370 Model). The photoluminescence (PL) spectra were measured using an excitation wavelength of 325 nm on a RF-1501 Shimadzu spectrophotometer.

Photocatalytic Activity

The photocatalytic activity of Ba-α-Bi_2O_3-γ-Fe_2O_3 nanocomposite was checked under sunlight irradiation in summer (GPS coordinates: N = 36°18' 41.6″, E = 59°31' 54.2″) and the AMX solution was used as a typical pharmaceutical pollutant (chemical structure is shown in Table 1).

A total of 50 ml of AMX solution (25 mg l^{-1}) containing 0.05 g of Ba-α-Bi_2O_3-γ-Fe_2O_3 nanocomposite was irradiated by sunlight. The experiments were carried out into a water-jacketed reactor maintained at 25± 2 °C with the initial pH = 5.7. It should be mentioned that before irradiation, the samples were placed in the dark for 15 min to obtain equilibrium adsorption-desorption between AMX and photocatalyst. The adsorption capacity of Ba-α-Bi_2O_3-γ-Fe_2O_3 nanocomposite was 4.13 mg l^{-1}. Samples from the suspensions of AMX and photocatalyst were removed frequently and separated from aqueous solution by a magnetic field. Then, the supernatant in phosphate buffer 7.2 was analyzed for the degradation of amoxicillin using a UV-Vis spectrophotometer at λ = 231 nm. For comparison, the experiments of photocatalytic activity were studied with γ-Fe_2O_3, α-Bi_2O_3 and α-Bi_2O_3-γ-Fe_2O_3. The TOC of the Ba-α-Bi_2O_3-γ-Fe_2O_3 nanocomposite was measured by a TOC-V CPH (model Shimadzu) analyzer after removing the photocatalysts by a magnet from them.

RESULTS AND DISCUSSION

XRD Analysis

Figure 1 shows the XRD patterns of the samples Ba-α-Bi_2O_3-γ-Fe_2O_3, α-Bi_2O_3, and γ-Fe_2O_3. The peaks of Bi_2O_3

Table 1. Chemical Characteristics of AMX

Drug	Chemical structure	Molecular weight ($g\ mol^{-1}$)	λ_{max} (nm)	pK_a
Amoxicillin	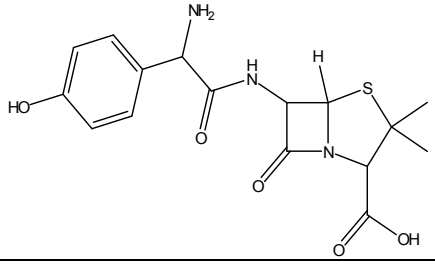	365.40	231	2.4 and 7.2

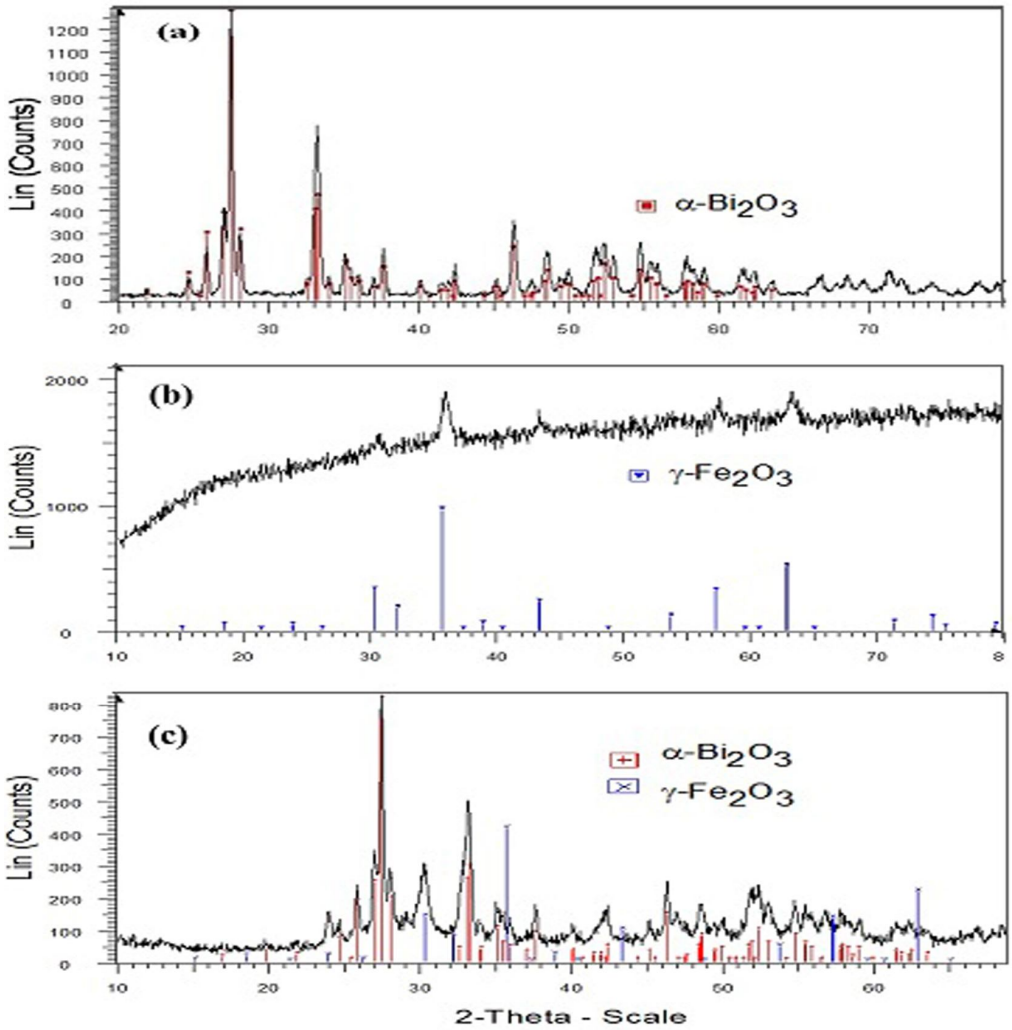

Fig. 1. X-ray diffraction patterns of the samples (a) α-Bi_2O_3, (b) γ-Fe_2O_3, (c) Ba-α-Bi_2O_3-γ-Fe_2O_3.

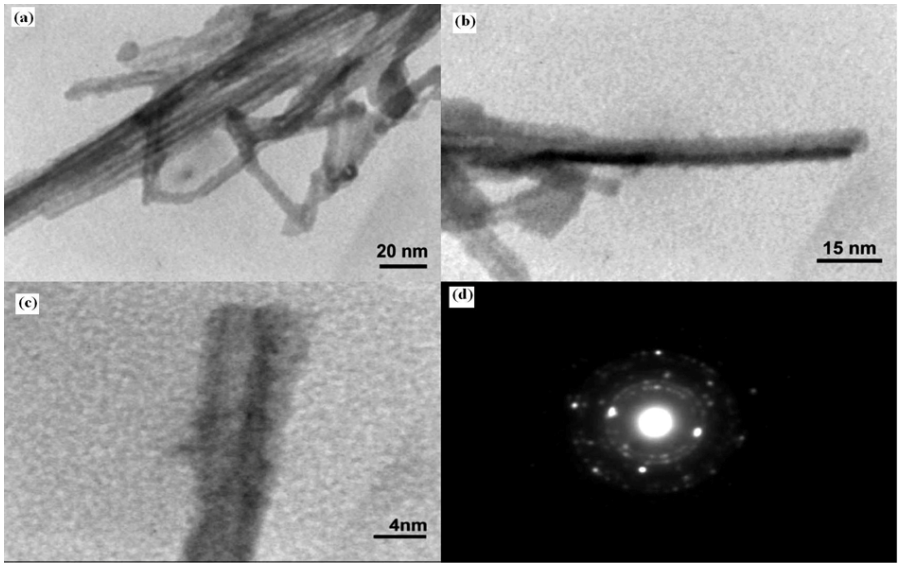

Fig. 2. Images (a, b) TEM, (c) HRTEM and (d) SAED of Ba-α-Bi_2O_3-γ-Fe_2O_3.

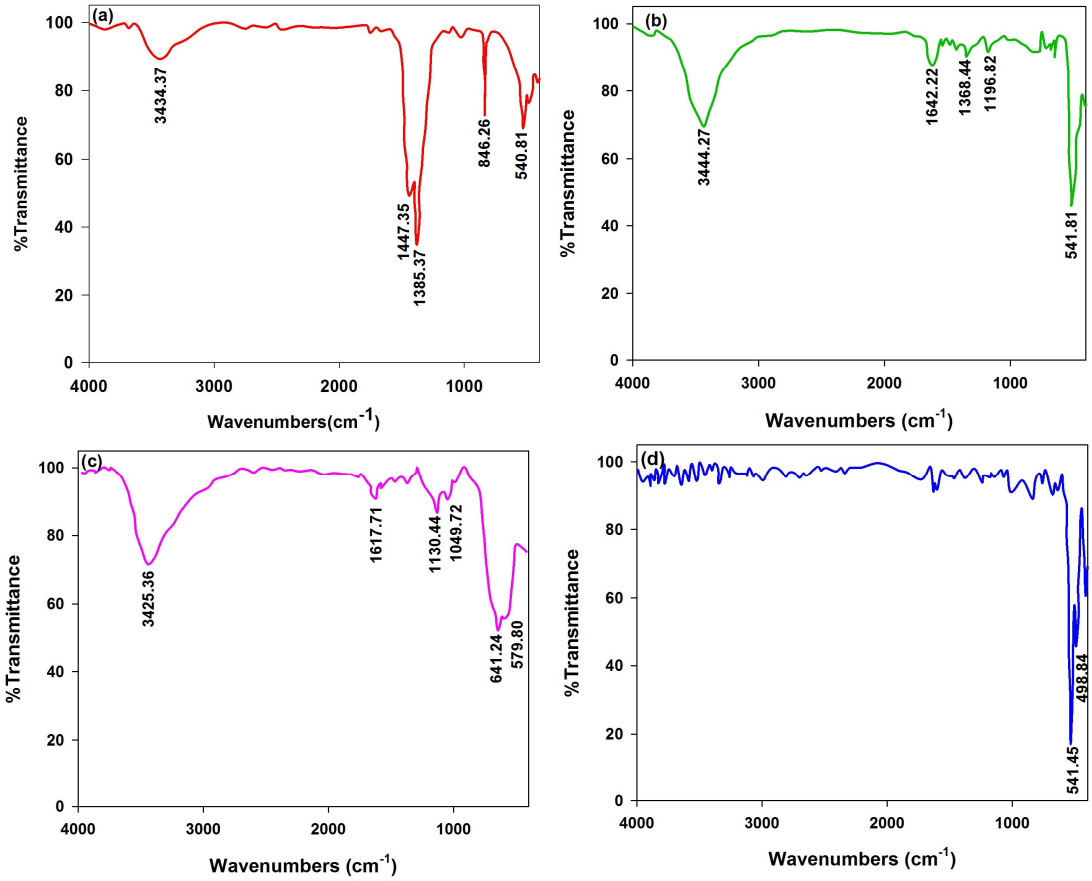

Fig. 3. FT-IR spectra of: a) γ-Fe_2O_3, b) α-Bi_2O_3, c) Ba-α-Bi_2O_3-γ-Fe_2O_3 nanocomposite, and d) α-Bi_2O_3-γ-Fe_2O_3.

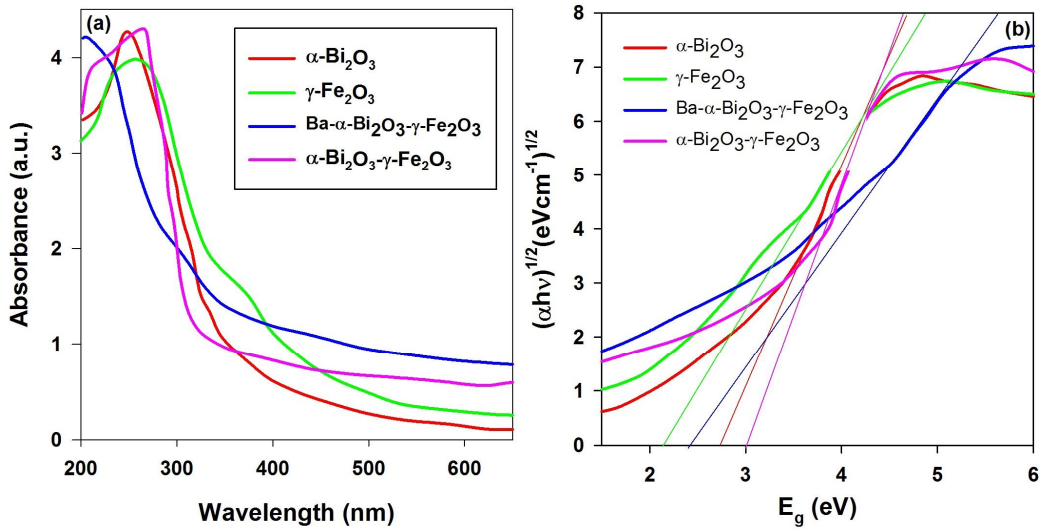

Fig. 4. a) UV-Vis spectra of Ba-α-Bi_2O_3-γ-Fe_2O_3 nanocomposite, α-Bi_2O_3-γ-Fe_2O_3, α-Bi_2O_3, and γ-Fe_2O_3.

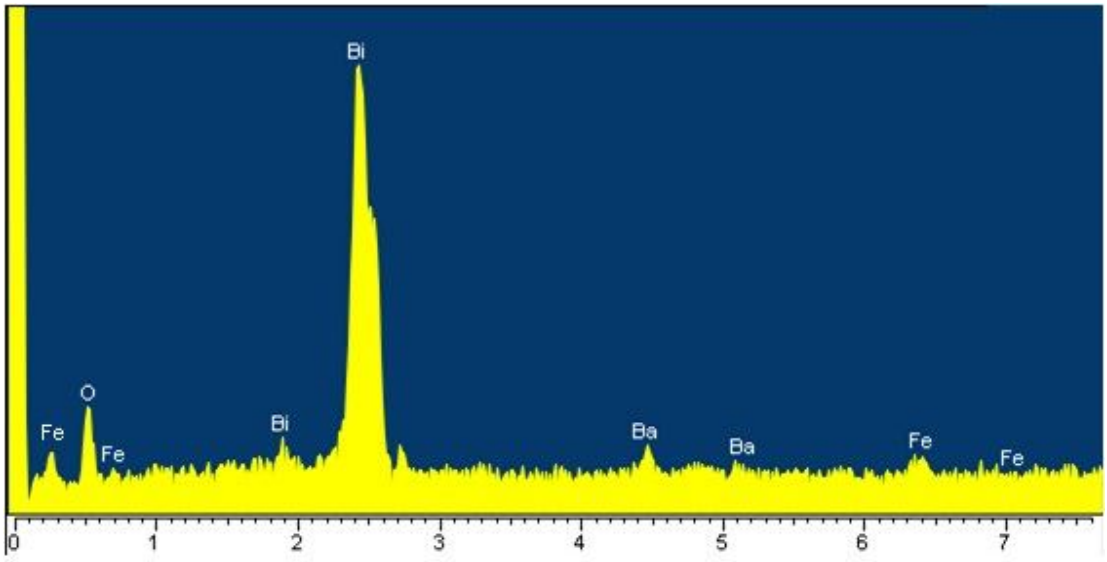

Fig. 5. The energy-dispersive X-ray (EDX) of the Ba-α-Bi_2O_3-γ-Fe_2O_3 nanocomposite.

nanoparticles and as-synthesized nanocomposite (Fig. 1a and c) at angles 2θ = 25.74°, 27.38°, 33.15°, 37.6°, 46.33°, 48.54°, and 54.79° can be indexed to the (002), (121), (202), (113), (223), (104) and (241) planes of the monoclinic α-Bi_2O_3 (JCPDS NO.27-0053). In addition, as shown in Fig. 1c, the weak peaks in nanocomposite at 2θ values of 23.97 and 30.36 can be assigned to the (210), (220) planes of γ-Fe_2O_3 (JCPDS ID: 24-0084) according to Fig. 1b. On other hand, in Fig. 1c, the peaks at 23.90°, 34.0°, 42.19° and 46.78° (2θ) can be attributed to the formation of BaO within the synthesis of nanocomposite which finally converted to $BaCO_3$ [48]. Therefore, the addition of Ba as

an impurity has been led to the decrease of peak intensity because of formation of oxygen vacancies due to charge and ionic size effects [49].

Particle Morphology

The microscopic structure of the photocatalyst was investigated by TEM and HRTEM. As seen in Fig. 2a and b, Ba-α-Bi_2O_3-γ-Fe_2O_3 nanocomposites are rods with diameters of 10-12 nm and lengths of 100-200 nm. The γ-Fe_2O_3 nanoparticles have been deposited as a regular row on the α-Bi_2O_3 surface. In comparison with α-Bi_2O_3 nanoparicles prepared by Wang *et al.* under ultrasound (diameters of 450-700 nm and lengths of 1-2.5 μm) [1] the synthesized nanocomposite is more regular with very small diameters. The difference may be due to the addition of Ba which can reduce the particle size. The particle size reduction has been reported in modified nanoparticles by others [35,36,48,50]. The size reduction could be attributed to the restricted crystal growth resulting from substituting of divalent Ba^{2+} instead of trivalent Bi^{3+} ions. Therefore, the substitution Ba^{2+} plays an important role in controlling size and morphology. Several diffraction rings in the SAED pattern, shown in Fig. 2d, confirm that the sample is polycrystalline.

FT-IR Spectra

Figure 3 shows the FT-IR spectra of γ-Fe_2O_3, α-Bi_2O_3, α-Bi_2O_3-γ-Fe_2O_3 and Ba-α-Bi_2O_3-γ-Fe_2O_3 to distinguish their functional groups. The bands at 3425 cm^{-1} and 1642 cm^{-1} are related to the stretching vibrations of O-H water molecules or hydroxyl groups and bending vibrations of water molecules, respectively. In Fig. 3a, two peaks at 641.24 cm^{-1} and 579.80 cm^{-1} correspond to vibrations of Fe-O [51]. According to Fig. 3b, the peaks at 1368.44 cm^{-1}, 1196.82 cm^{-1} and 541.81 cm^{-1} are attributed to the stretching vibrations of NO_3^- groups, Bi-O-Bi and bending vibrations of Bi-O, respectively [52]. In the spectrum related to the nanocomposite (Fig. 3c), the new peak at about 1447.35 cm^{-1} is attributed to the vibrations of barium carbonate [53]. This peak was not observed in α-Bi_2O_3-γ-Fe_2O_3 (Fig. 3d).

UV-Vis Analysis

Figure 4 shows the UV-Vis spectra of the Ba-α-Bi_2O_3-γ-Fe_2O_3 nanocomposite, α-Bi_2O_3-γ-Fe_2O_3, γ-Fe_2O_3, and α-Bi_2O_3. According to this figure, the synthesized nanocomposite is more sensitive to sunlight than other samples. The band gap energies of the samples was determined by the Tauc equation [18]. The band gap calculated for the nanocomposite, α-Bi_2O_3-γ-Fe_2O_3, γ-Fe_2O_3, and α-Bi_2O_3 was about 2.5, 2.9, 2.1, and 2.7 eV, respectively.

EDX and VSM Analysis

The composition of the nanocomposite was further investigated by EDX. The EDX pattern in Fig. 5 confirms that photocatalyst is composed of the elements of Bi, Fe, O and Ba. Also, in order to explain the magnetic property of Ba-α-Bi_2O_3-γ-Fe_2O_3 nanocomposite, the magnetic hysteresis curve was measured at room temperature, as indicated in Fig. 6. The hysteresis loop exhibits ferromagnetic behavior with saturation magnetization (M_s) of 2.59 emu g^{-1}.

Photocatalytic Degradation of Amoxicillin

The photocatalytic activity of the Ba-α-Bi_2O_3-γ-Fe_2O_3 nanocomposite, α-Bi_2O_3- γ-Fe_2O_3, γ-Fe_2O_3, and α-Bi_2O_3 was investigated on AMX under sunlight irradiation (Fig. 7). According to Fig. 7, AMX cannot be degraded under sunlight irradiation without photocatalyst. On the basis of the results obtained, the Ba-α-Bi_2O_3-γ-Fe_2O_3 nanocomposite has the highest effect on the degradation of the AMX in comparison with other samples. These results can be confirmed by PL too. Figure 8 shows the PL spectra of the synthesized nanoparticles with the excitation wavelength at 350 nm. A strong broad emission peak at around 430 nm and several peaks in the range of 400-500 nm are found in the PL spectra. The PL intensity of the samples follows the order: α-Bi_2O_3 > α-Bi_2O_3-γ-Fe_2O_3 > γ-Fe_2O_3 > Ba-α-Bi_2O_3-γ-Fe_2O_3. Therefore, Ba-α-Bi_2O_3-γ-Fe_2O_3 nanocomposite prepared under ultrasound shows the lowest intensity indicating the efficient separation rate of the carriers in nanocomposite structure. In addition, the synthesized nanocomposite in this work as a photocatalyst is more effective in degradation of AMX than the works presented in the literature (Table 2). The higher photocatalytic activities of the sample synthesized via ultrasound could be attributed to its smaller nano-crystallite size and higher surface area. This means that the number of sorption sites

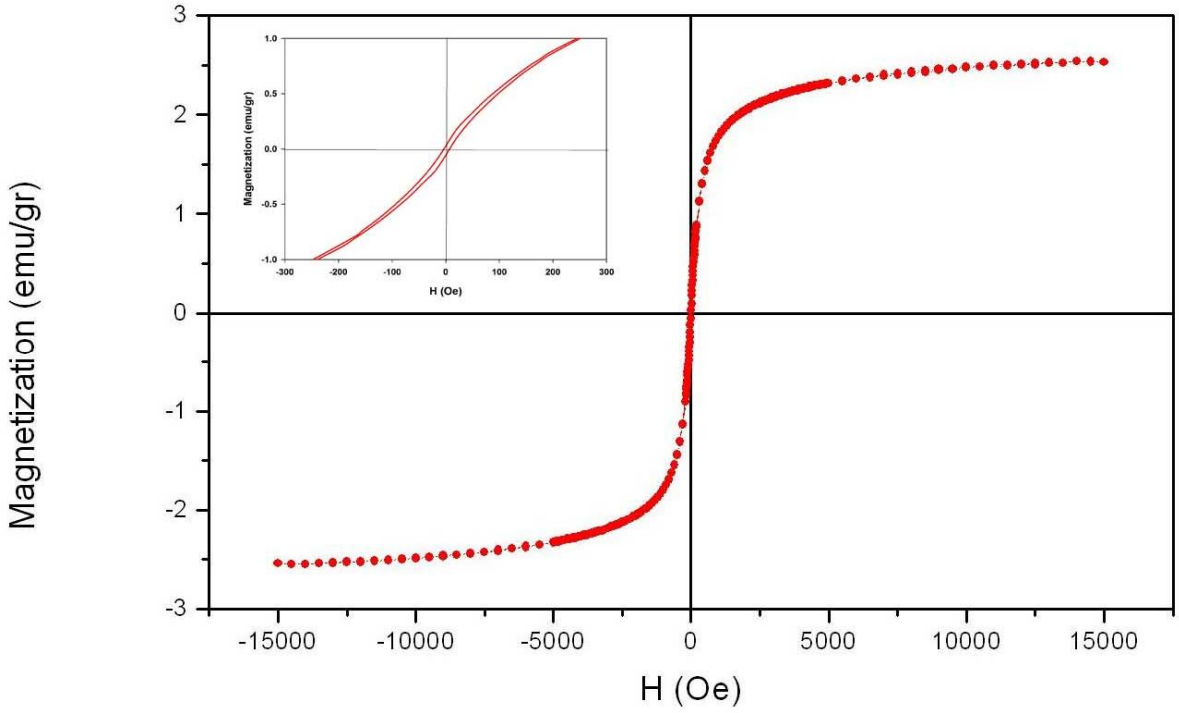

Fig. 6. The magnetization curve of Ba-α-Bi_2O_3-γ-Fe_2O_3 nanocomposite.

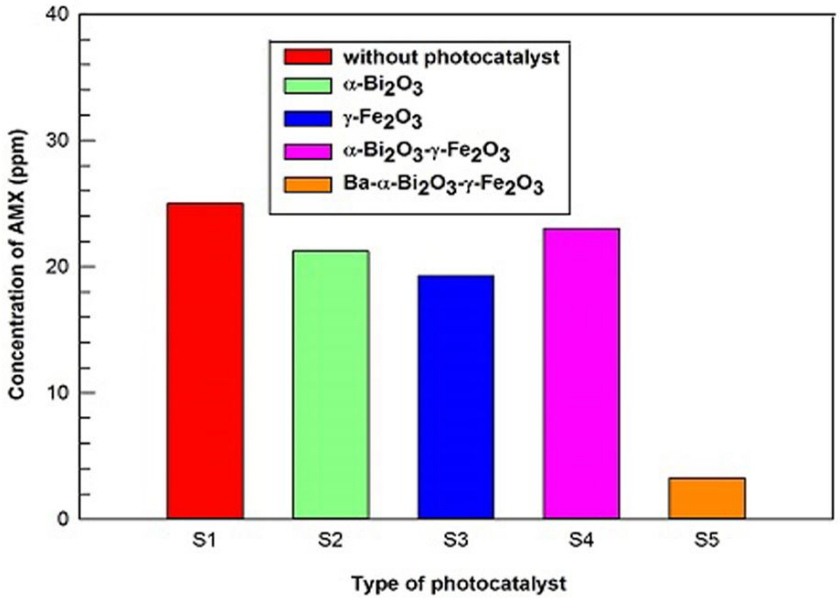

Fig. 7. Concentration reduction of AMX in the presence of different nanophotocatalysts ($[C]_0$: 25 mg l^{-1}, 0.05 g catalyst, pH = 5.7, 25 °C, 2 h).

Table 2. Comparison of Different Photocatalysts Applied for the Degradation of AMX

Type of photocatalyst	Initial concentration of AMX (mg l^{-1})	Time irradiation (min)	Degradation	Mineralization	Ref.
Photo-Fenton	4.5	120	0	-	[44]
UV/ZnO	200	300	44.2%	18.4%	[11]
UV-A/TiO_2	10	90	0	90%	[55]
UV/TiO_2	200	350	70%	-	[56]
UV	200	350	10%	-	[56]
UV/H_2O_2/TiO_2	104	300	-	12.3%	[46]

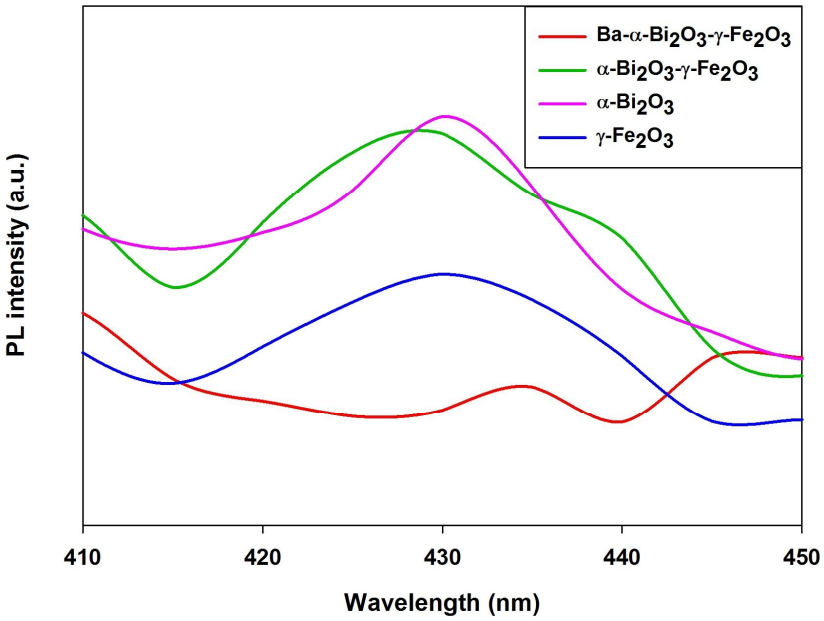

Fig. 8. PL spectra of different samples.

and the radical species were increased by applying ultrasound in the synthesis of nanocomposite. In addition, rising the temperature and pressure during the asymmetric collapse, provide a favorable environment for the growth of nanocrystals [54].

Figure 9 shows the UV-Vis spectra of AMX during its degradation by Ba nanocomposite at different interval times. As it is observed, AMX was mostly degraded in 2 h, and the TOC measurements showed that AMX has been mineralized to about 55% (TOC for the parent sample and the degraded sample were 10.62 mg l^{-1} and 5.40 mg l^{-1}, respectively).

The presence of Ba into the nanocomposite lattice caused defects and oxygen vacancies that they can become

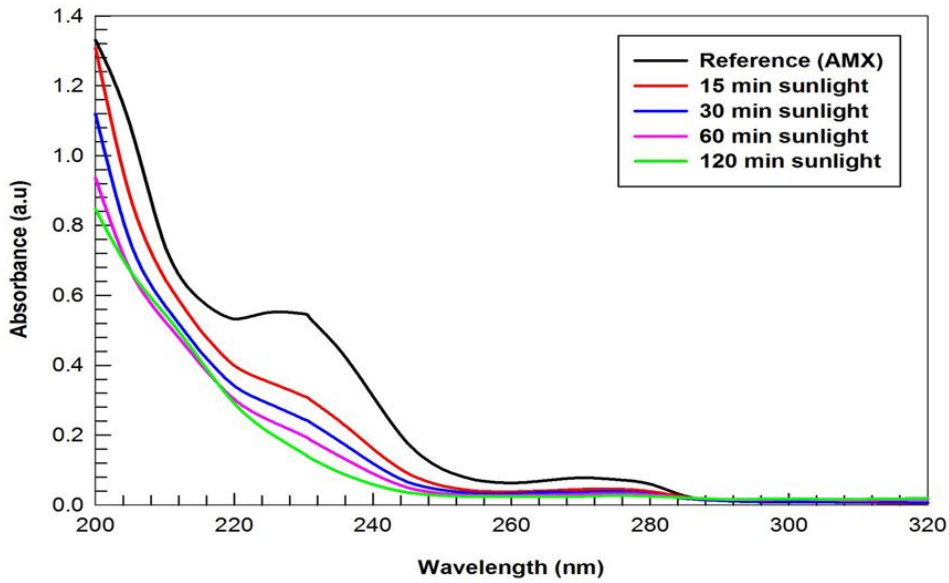

Fig. 9. UV-Vis absorption spectra of amoxicillin versus time in the presence of nanocomposite Ba-α-Bi_2O_3-γ-Fe_2O_3 ($[C]_0$: 25 mg l^{-1}, 0.05 g catalyst, pH = 5.7, 25 °C).

Table 3. Apparent Rate Constants of AMX Degradation in the Presence of Different Photocatalysts and Corresponding $t_{0.5}$

Photocatalyst	k_{app} (min^{-1})	$t_{0.5}$ (min)
without photocatalyst	0.0009	770.1
α-Bi_2O_3	0.0016	433.2
γ-Fe_2O_3	0.0029	239.0
α-Bi_2O_3-γ-Fe_2O_3	0.0012	577.6
Ba-α-Bi_2O_3-γ-Fe_2O_3	0.0170	40.7

centered to capture photo-induced electrons and prevent of recombination electron-hole pairs. This leads to increase the photocatalytic activity of Ba-α-Bi_2O_3-γ-Fe_2O_3 nanocomposite [35]. Consequently, the degradation will be mainly due to the active species produced during the photocatalytic process such as hydroxyl radical, hole and superoxide ion [46]. In addition, the decrease of degradation may be due to the presence of interfering anions such as sulfate anions [46,57].

From kinetic studies on photocatalytic reactions of nanocomposite, the reaction can be explained in accordance with pseudo-first-order model (Eq. (1)):

$$\ln\frac{C}{C_0} = -k_{app}t \qquad (1)$$

where k_{app} is the apparent reaction rate constant, t the

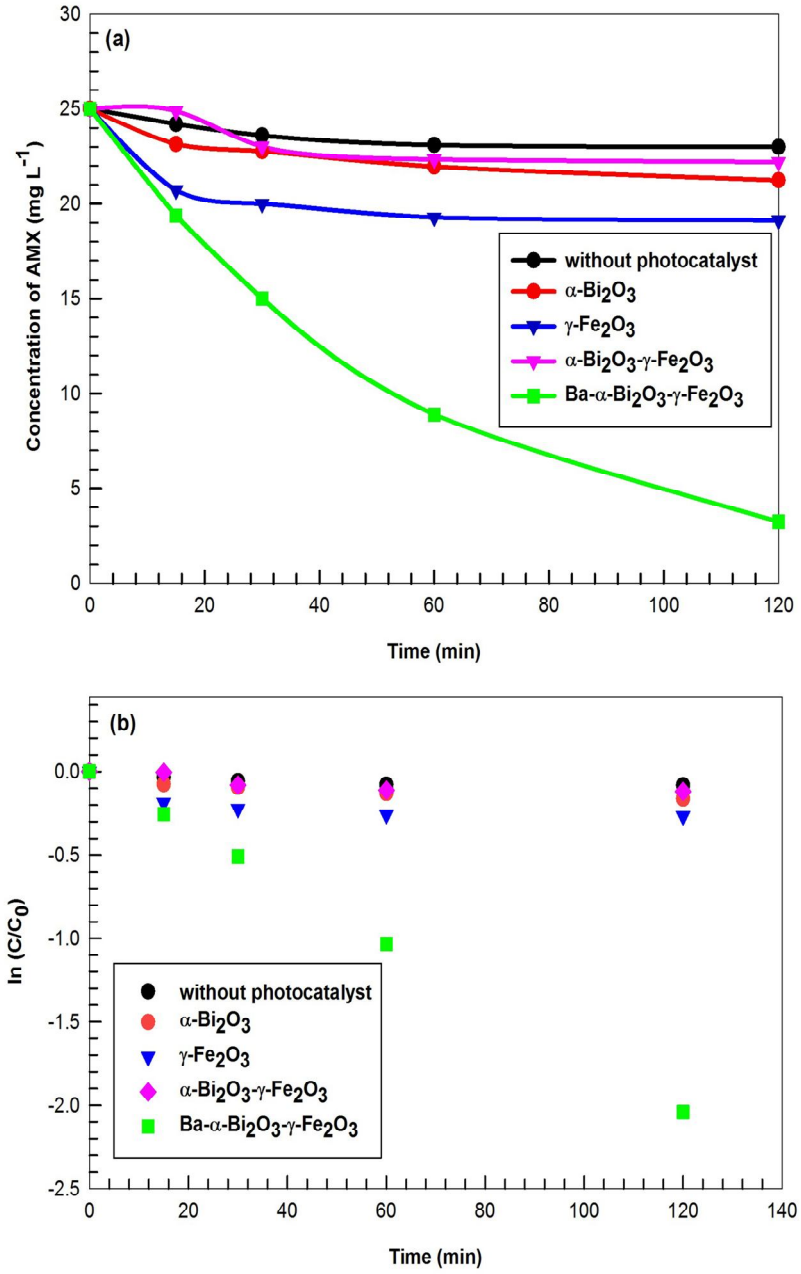

Fig. 10. a) Concentration reduction of AMX in the presence of different nanophotocatalysts, b) Pseudo firstorderkinetics fo r photodegradation of AMX in the presence of different nanophotocatalysts ($[C]_0$: 25 mg l^{-1}, 0.05 g catalyst, pH = 5.7, 25°C).

reaction time, C_0 the initial concentration of AMX in aqueous solution and C is the residual concentration of the AMX at t time. The value of k_{app} was determined from the slope of the graph plotted $\ln(C/C_0)$ versus the reaction time.

Figs. 10a and b show the concentration reduction of AMX in the presence of different nanophotocatalysts. The rate of degradation of AMX under solar light irradiation was found to obey the first order kinetics model. Table 3 contains the

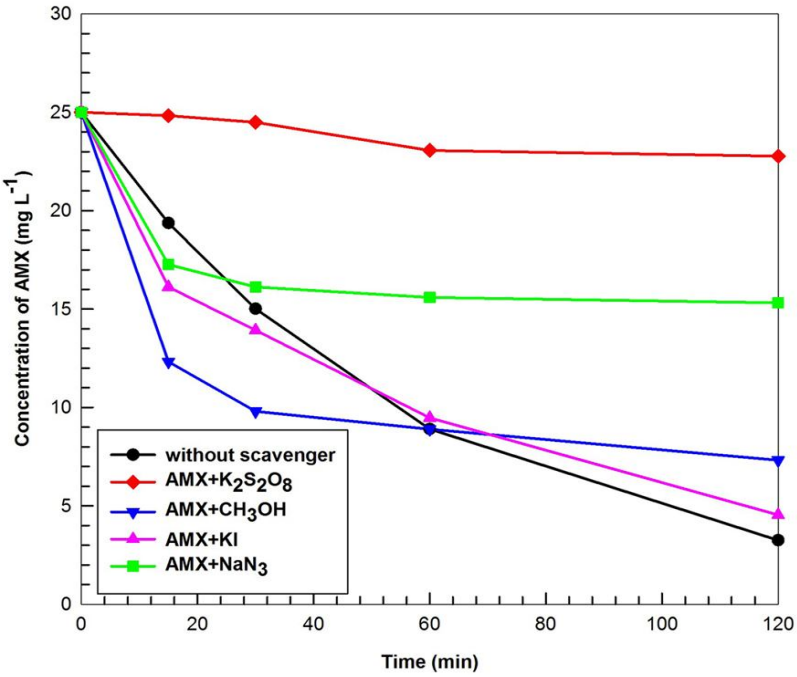

Fig. 11. The effect of scavengers in the degradation of AMX ($[C]_0$: 25 mg l^{-1}, 0.05 g catalyst, pH = 5.7, 25°C).

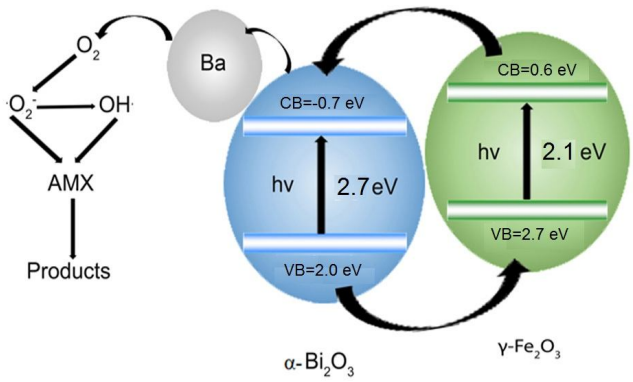

Fig. 12. Schematic illustration for the charge separation and transfer process in the nanocomposite of Ba-α-Bi_2O_3-γ-Fe_2O_3 for the degrading of AMX under sunlight irradiation.

calculated k_{app} and $t_{1/2}$ by comparing the obtained rate constants from Fig. 10.

The Proposed Mechanism for the Photocatalytic Activity of Ba-α-Bi_2O_3-γ-Fe_2O_3 Nanocomposite

It has been reported that the h^+, $OH^{\bullet}$ and e^- are the major reactive species for the photocatalytic oxidation. To investigate the photocatalytic mechanisms of the Ba-α-Bi_2O_3-γ-Fe_2O_3 nanocomposite, several scavengers were used to explore the reactive species in the process of degradation. Addition of different scavengers into the reaction solutions led to the change of photocatalytic

efficiency. In this study, potassium iodide (KI), methanol (CH_3OH), sodium azide (NaN_3), and potassium persulfate ($K_2S_2O_8$) were used as the scavengers for the hole (h^+), hydroxyl radical ($OH^\bullet$), singlet oxygen ($^1O_2$), and electron (e^-), respectively (Fig. 11).

By adding $K_2S_2O_8$ (2.5 mM), the photodegradation was strongly inhibited, indicating that the process of degradation was mainly proceeded by direct interaction of AMX with e^-. On the other hand, addition of methanol (2.5 mM) was led to slight decrease of the decomposition of AMX due to low generation of $OH^\bullet$ in the solution. In addition, the photodegradation of AMX was almost invariable in the presence of KI (2.5 mM). Hence, hole is not the major reactive species. However, by addition of sodium azide as a $^1O_2$ scavenger, the degradation of AMX decreased as shown in Fig. 10. On the basis of the results, it is clear that e^-, $^1O_2$ and $OH^\bullet$ are the major reactive species in the photocatalytic degradation of AMX by Ba-α-Bi_2O_3-γ-Fe_2O_3 as a photocatalyst.

It is also possible to demonstrate the degradation process based on the energy levels of the components of the nanocomposite. The positions of the valence band (VB) edge of γ-Fe_2O_3 and α-Bi_2O_3 are located at 2.7 eV and 2.0 eV, respectively. The conduction band (CB) positions of γ-Fe_2O_3 and α-Bi_2O_3 can be calculated by the following empirical equation:

$$E_{CB} = E_{VB} - E_g \tag{2}$$

where E_{VB} is the VB potential and E_{CB} is the CB potential. The position of the CB edges of γ-Fe_2O_3 and α-Bi_2O_3 are located at 0.6 eV and -0.7 eV, respectively.

On the basis of the results, it was confirmed that electrons have major responsibility for the formation of active species such as singlet oxygen in the degradation of AMX. Hence, the proposed mechanism can explain the enhancement of the photocatalytic properties of the Ba-α-Bi_2O_3-γ-Fe_2O_3 nanocomposite. The conduction band of α-Bi_2O_3 is more positive than that of γ-Fe_2O_3 and could act as a sink for the photo-generated electrons from the surface of γ-Fe_2O_3. Similarly, the photo-induced holes on the α-Bi_2O_3 surface migrate to γ-Fe_2O_3, as shown in Fig. 12.

CONCLUSIONS

Novel nanocomposite Ba-α-Bi_2O_3-γ-Fe_2O_3 was synthesized by sonication method successfully and was characterized by XRD, TEM, HRTEM, UV-Vis, FTIR, EDX, VSM and PL. The results showed that the synthesized nanocomposite containing crystalline phases with rod shape and a band gap of 2.5 eV. The photocatalytic degradation of AMX was carried out by the Ba nanocomposite and the degradation was completed in 6 h under visible light irradiation. The TOC measurements showed that AMX has been mineralized to about 55% in 2 h. Our results indicate that Ba-α-Bi_2O_3-γ-Fe_2O_3 nano-rods would be a good candidate as visible light photocatalyst for the degradation of similar pollutants. The photocatalytic degradation was fitted to the pseudo-first-order kinetics model. The enhanced photocatalytic performance of nanocomposite can be attributed to the formation of oxidative species such as $^1O_2$ and $OH^\bullet$ in the solution by electrons on the catalyst surface.

ACKNOWLEDGMENT

The authors acknowledge the help given by Mr Daliyani from Solid State Physics Research Center, Damghan University. The support of Ferdowsi University of Mashhad (Research and Technology) is appreciated for the project (3/20243, 17/12/2011).

REFERENCES

[1] Zhang, L.; Wang, W.; Yang, J.; Chen, Zh.; Zhang, W.; Zhou, L.; Liu, Sh., Sonochemical synthesis of nanocrystallite Bi2O3 as a visible-light-driven photocatalyst. *Appl. Catal. A* **2006**, *308*, 105-110, DOI: 10.1016/j.apcata.2006.04.016.

[2] Mou, F.; Xu, L.; Ma, H.; Guan, J.; Chen, D.; Wang, Sh., Facile preparation of magnetic γ-Fe_2O_3/TiO_2 janus hollow bowls with efficient visible-light photocatalytic activities by asymmetric shrinkage. *Nanoscale,* **2012**, *4*, 4650-4657, DOI: 10.1039/C2NR30733B.

[3] Peng, L.; Xie, T.; Lu, Y.; Fan, H.; Wang, D., Synthesis, photoelectric properties and photocatalytic activity of the Fe_2O_3/TiO_2 heterogeneous

photocatalysts. *Phys. Chem. Chem. Phys.,* **2010**, *12*, 8033-8041, DOI: 10.1039/C002460K.

[4] Abdullah, A. H.; Mun, L. K.; Zainal, Z.; Hussein, M. Z., Photo-degradation of chlorophenoxyacetic acids by ZnO/γ-Fe_2O_3 nanocatalysts: a comparative study. *Int. J. Chem.,* **2013**, *5*, 56-65, DOI: 10.5539/ ijc.v5n4p56.

[5] Jung, Y. J.; Kim, W. G.; Yoon, Y.; Kang, J. W.; Hong, Y. M.; Kim, H. W., Removal of amoxicillin by UV and UV/H_2O_2 processes. *Sci. Total Environ.,* **2012**, *420*, 160-167, DOI: 10.1016/ j.scitotenv.2011.12.011.

[6] Ananpattarachai, J.; Kajitvichyanukul, P.; Seraphin, S., Visible light absorption ability and photocatalytic oxidation activity of various interstitial N-doped TiO_2 prepared from different nitrogen dopants. *J. Hazard. Mater.,* **2009**, *168*, 253-261, DOI: 10.1016/ j.jhazmat.2009.02.036.

[7] Yang, L.; Hu, C.; Nie, Y.; Qu, J., Catalytic ozonation of selected pharmaceuticals over mesoporous alumina-supported manganese oxide. *Environ. Sci. Technol.,* **2009**, *43*, 2525-2529, DOI: 10.1021/ es803253c.

[8] Chatterjee, D.; Dasgupta, S., Visible light induced photocatalytic degradation of organic pollutants. *J. Photochem. Photobiol. C: Photochem. Rev.,* **2005**, *6*, 186-205, DOI: 10.1016/j.jphotochemrev.2005.09.001.

[9] Asahi, R.; Morikawa, T.; Ohwaki, T.; Taga, Y., Visible-light photocatalysis in nitrogen-doped titanium oxides. *Science,* **2001**, *293*, 269-271, DOI: 10.1126/science.1061051.

[10] Elmolla, E. S.; Chaudhuri, M., Degradation of the antibiotics amoxicillin, ampicillin and cloxacillin aqueous solution by the photo-fenton process. *J. Hazard. Mater.,* **2009**, *172*, 1476-1481, DOI: 10.1016/j.jhazmat.2009.08.015.

[11] Elmolla, E. S.; Chaudhuri, M., Degradation of amoxicillin, ampicillin and cloxacillin antibiotics in aqueous solution by the UV/ZnO photocatalytic process. *J. Hazard. Mater.,* **2010**, *173*, 445-449, DOI: 10.1016/j.jhazmat.2009.08.104.

[12] De, G. C.; Roy, A. M.; Bhattacharya, S. S., Effect of n-Si on the photocatalytic production of hydrogen by Pt-loaded CdS and CdSZnS catalyst. *Int. J. Hydrogen Energy,* **1996**, *21*, 19-23, DOI: 10.1016/0360-3199(95)00031-8.

[13] Hwang, D. W.; Kim, J.; Park, T. J.; Lee, J. S., Mg-doped WO_3 as a novel photocatalyst for visible light induced water splitting. *Catal. Lett.,* **2002**, *80*, 53-57, DOI: 10.1023/A:1015322625989.

[14] Cabot, A.; Marsal, A.; Arbiol, J.; Morante, J. R., Bi2O3 as a selective sensing material for NO detection. *Sens. Actuators B,* **2004**, *99*, 74-89, DOI: 10.1016/j.snb.2003.10.032.

[15] Shuk, P.; Wiemhöfer, H. D.; Guth, U.; Göpel, W.; Greenblatt, M., Oxide ion conducting solid electrolytes based on Bi_2O_3. *Solid State Ion.,* **1996**, *89*, 179-196, DOI: 10.1016/0167-2738(96)00348-7.

[16] Moens, L.; Ruiz, P.; Delmon, B.; Devillers, M., Enhancement of total oxidation of isobutene on bismuth-promoted tin oxide catalysts. *Catal. Lett.,* 1997, *46*, 93-99, DOI: 10.1023/A:1019050030865.

[17] Sammes, N. M.; Tompsett, G. A.; Näfe, H.; Aldinger, F., Bismuth based oxide electrolytes-structure and ionic conductivity. *J. Eur. Ceram. Soc.,* **1999**, *19*, 1801-1826, DOI: 10.1016/S0955-2219(99)00009-6.

[18] Pugazhenthiran, N.; Sathishkumar, P.; Murugesan, S.; Anandan, S., Effective degradation of acid orange 10 by catalytic ozonation in the presence of Au-Bi_2O_3 nanoparticles. *Chem. Eng. J.,* **2011**, *168*, 1227-1233, DOI: 10.1016/j.cej.2011.02.020.

[19] Gurunathan, K., Photocatalytic hydrogen production using transition metal ions-doped γ-Bi_2O_3 semiconductor particles. *Int. J. Hydrogen Energy,* **2004**, *29*, 933-940, DOI: 10.1016/ j.ijhydene.2003.04.001.

[20] Bessekhouad, Y.; Robert, D.; Weber, J. V., Photocatalytic activity of Cu_2O/TiO_2, Bi_2O_3/TiO_2 and $ZnMn_2O_4/TiO_2$ heterojunctions. *Catal. Today,* **2005**, *101*, 315-321, DOI: 10.1016/j.cattod.2005.03.038.

[21] Serpone, N.; Maruthamuthu, P.; Pichat, P.; Pelizzetti, E.; Hidaka, H., Exploiting the interparticle electron transfer process in the photocatalysed oxidation of phenol, 2-chlorophenol and pentachlorophenol: Chemical evidence for electron and hole transfer between coupled semiconductors. *J. Photochem. Photobiol. A: Chem.,* **1995**, *85*, 247-255, DOI: 10.1016/1010-6030(94)03906-B.

[22] Liu, R.; Ye, H.; Xiong, X.; Liu, H., Fabrication of TiO_2/ZnO composite nanofibers by electrospinning and their photocatalytic property. *Mater. Chem. Phys.,* **2010**, *121*, 432-439, DOI: 10.1016/ j.matchemphys.2010.02.002.

[23] Zheng, L. R.; Zheng, Y. H.; Chen, C. Q.; Zhan, Y. Y.; Lin, X. Y.; Zheng, Q.; Zhu, J. F., Network structured SnO_2/ZnO heterojunction nanocatalyst with high photocatalytic activity. *Inorg. Chem.,* 2009, *48*, 1819-1825, DOI: 10.1021/ic802293p.

[24] Li, L. Z.; Yan, B., $BiVO_4/Bi_2O_3$ submicrometer sphere composite: Microstructure and photocatalytic activity under visible-light irradiation. *J. Alloy Compd.,* **2009**, *476*, 624-628, DOI: 10.1016/ j.jallcom.2008.09.083.

[25] Chai, S. Y.; Kim, Y. J.; Jung, M. H.; Chakraborty, A. K.; Jung, D.; Lee, W. I., Heterojunctioned BiOCl/Bi2O3, a new visible light photocatalyst. *J. Catal.,* **2009**, *262*, 144-149, DOI: 10.1016/ j.jcat.2008.12.020.

[26] Zhang, H. T.; Ouyang, S. X.; Li, Z. S.; Yu, L. F.; Liu, T.; Ye, J. H.; Zou, Z., Preparation, characterization and photocatalytic activity of polycrystalline $Bi_2O_3/SrTiO_3$ composite powders. *J. Phys. Chem. Solids,* **2006**, *67*, 2501-2505, DOI: 10.1016/ j.jpcs.2006.07.005.

[27] Neppolian, B.; Kim, Y.; Ashokkumar, M.; Yamashita, M.; Choi, H., Preparation and properties of visible light responsive $ZrTiO_4/Bi_2O_3$ photocatalysts for 4-chlorophenol decomposition. *J. Hazard. Mater.,* **2010**, *182*, 557-562, DOI: 10.1016/j.jhazmat.2010.06.069.

[28] Li, L. Z.; Yan, B., CeO_2-Bi_2O_3 nanocomposite: Two step synthesis, microstructure and photocatalytic activity. *J. Noncryst. Solids,* **2009**, *355*, 776-779, DOI: 10.1016/j.jnoncrysol.2009.04.003.

[29] Hameed, A.; Gombac, V.; Montini, T.; Mauro, G.; Fornasiero, P., Synthesis, characterization and photocatalytic activity of NiO-Bi_2O_3 nanocomposites. *Chem. Phys. Lett.,* **2009**, *472*, 212-216, DOI: 10.1016/j.cplett.2009.03.017.

[30] Jun, S.; Wen, Z.; Weichang, H.; Xin, X.; Huaizhe, X.; Tianmin, W., Visible-light photocatalytic properties of γ-Bi_2O_3 composited with Fe_2O_3. *Rare Metals,* **2011**, *30*, 140-143, DOI: 10.1007/s12598-011-0256-y.

[31] Ziolo, R. F.; Giannelis, E. P.; Weinstein, B. A.; Ohoro, M. P.; Ganguly, B. N.; Mehrotra, V.; Russell, M. W.; Huffman, D. R., Matrix-mediated synthesis of nanocrystalline γ-Fe_2O_3: A new optically transparent magnetic material. *Science,* **1992**, *257*, 219-223, DOI: 10.1126/science.257.5067.219.

[32] Du, W. P.; Xu, Y. M.; Wang, Y. S., Photoinduced degradation of orange II on different iron (hydr) oxides in aqueous suspension: rate enhancement on addition of hydrogen peroxide, silver nitrate, and sodium fluoride. *Langmuir,* **2008**, *24*, 175-181, DOI: 10.1021/la7021165.

[33] Leland, J. K.; Bard, A. J., Photochemistry of colloidal semiconducting iron oxide polymorphs. *J. Phys. Chem.,* **1987**, *91*, 5076-5083, DOI: 10.1021/ j100303a039.

[34] Hardee, K. L.; Bard, A. J., Semiconductor electrodes: X-photoelectrochemical behavior of several polycrystalline metal oxide electrodes in aqueous solutions. *J. Electrochem. Soc.,* **1977**, *124*, 215-224, DOI: 10.1149/1.2133269.

[35] Li, J.; Cai, D.; Song, J.; Jin, D.; Yu, Sh.; Cheng, J., Synthesis and photocatalytic property of Ba-doped BiFeO3 nanoparticles. IEEE International Symposium on the Applications of Ferroelectrics (ISAF), 2010, 1-4, DOI: 10.1109/ISAF.2010.5712271.

[36] Bhushan, B.; Basumallick, A.; Bandopadhyay, S. K.; Vasanthacharya, N. Y.; Das, D., "Effect of alkaline earth metal doping on thermal, optical, magnetic and dielectric properties of $BiFeO_3$ nanoparticles". *J. Phys. D: Appl. Phys.,* **2009**, *42*, 1-8.

[37] Roth, R. S.; Hwang, N. M.; Rawn, C. J.; Burton, B. P.; Ritter, J. J., Phase equilibria in the systems CaO-CuO and CaO- Bi_2O_3. *J. Am. Ceram. Soc.,* **1991**, *74*, 2148-2151, DOI: 10.1111/j.1151-2916.1991.tb08274.x.

[38] Helaïli, N.; Bessekhouad, Y.; Bouguelia, A.; Trari, M., Visible light degradation of Orange II using CuyOz/TiO_2 heterojunctions. *J. Hazard. Mater.,* **2009**, *168*, 484-492, DOI: 10.1016/j.jhazmat.2009.02.066.

[39] Talebian, A.; Entezari, M. H.; Ghows, N., Complete mineralization of surfactant from aqueous solution by a novel sono-synthesized nanocomposite (TiO_2-Cu_2O) under sunlight irradiation. *Chem. Eng. J.,* **2013**, *229*,

304-312, DOI: 10.1016/j.cej.2013.05.117.

[40] Taherian, S.; Entezari, M. H.; Ghows, N., Sono-catalytic degradation and fast mineralization of p-chlorophenol: La0.7Sr0.3MnO_3 as a nano-magnetic green catalyst. *Ultrason. Sonochem.,* **2013**, *20*, 1419-1427, DOI: 10.1016/j.ultsonch.2013.03.009.

[41] Gozlan, I.; Rotstein, A.; Avisar, D., Amoxicillin-degradation products formed under controlled environmental conditions: Identification and determination in the aquatic environment. *Chemosphere,* **2013**, *91*, 985-992, DOI: 10.1016/j.chemosphere.2013.01.095.

[42] Tiehm, A.; Krabnitzer, S.; Koltypin, Y.; Gedanken, A., Chloroethene dehalogenation with ultrasonically produced air-stable nano iron. *Ultrason. Sonochem.,* **2009**, *16*, 617-621, DOI: 10.1016/j.ultsonch.2009.01.005.

[43] Trovo, A. G.; Nogueira, R. F. P.; Agüera, A.; Fernandez-Alba, A. R.; Malato, S., Degradation of the antibiotic amoxicillin by photo-Fenton process-Chemical and toxicological assessment. *Water Res.,* **2011**, *45*, 1394-1402, DOI: 10.1016/j.watres.2011.10.029.

[44] Homem, V.; Alves, A.; Santos, L., Amoxicillin degradation at ppb levels by Fenton's oxidation using design of experiments. *Sci. Total Environ.,* **2010**, *408*, 6272-6280, DOI: 10.1016/j.scitotenv.2010.08.058.

[45] Klauson, D.; Babkina, J.; Stepanova, K.; Krichevskaya, M.; Preis, S., Aqueous photocatalytic oxidation of amoxicillin. *Catal. Today,* **2010**, *151*, 39-45, DOI: 10.1016/j.cattod.2010.01.015.

[46] Elmolla, E. S.; Chaudhuri, M., Photocatalytic degradation of amoxicillin, ampicillin and cloxacillin antibiotics in aqueous solution using UV/TiO_2 and UV/H_2O_2/TiO_2 photocatalysis. *Desalination,* **2010**, *252*, 46-52, DOI: 10.1016/j.desal.2009.11.003.

[47] Afkhami, A.; Moosavi, R., Adsorptive removal of Congo red, a carcinogenic textile dye, from aqueous solutions by maghemite nanoparticles. *J. Hazard. Mater.,* **2010**, *174*, 398-403, DOI: 10.1016/j.jhazmat.2009.09.066.

[48] Venkatachalam, N.; Palanichamy, M.; Arabindoo, B.; Murugesan, V., Alkaline earth metal doped nanoporous TiO_2 for enhanced photocatalytic mineralisation of bisphenol-A. *Catal. Com.,* **2007**, *8*, 1088-1093, DOI: 10.1016/j.catcom.2006.10.025.

[49] Nunn, S. D.; Pazant, E. A., Properties of ionic conducting β-Bi_2O_3 containing mixed dopants. *J. Am. Ceram. Soc.,* **2002**, *85*, 2633-2636, DOI: 10.1111/1151-2916.2002.tb00506.x.

[50] Soitah, T. N.; Yang, Ch., Effect of Fe^{3+} doping on structural, optical and electrical properties δ-Bi_2O_3 thin films. Current *Appl. Phys.,* **2010**, *10*, 724-728, DOI: 10.1016/j.cap.2009.06.060.

[51] Gao, Q.; Chen, F.; Zhang, J.; Hong, G.; Ni, J.; Wei, X.; Wang, D., The study of novel Fe_3O_4/γ-Fe_2O_3 core/shell nanomaterials with improved properties. *J. Magnetism. Magnet. Mater.,* **2009**, *321*, 1052-1057, DOI: 10.1016/j.jmmm.2008.10.022.

[52] Li, W., Facile synthesis of mono disperse Bi2O3 nanoparticles. *Mater. Chem. Phys.,* **2006**, *99*, 174-180, DOI: 10.1016/j.matchemphys.2005.11.007.

[53] Kaur, T.; Srivastava, A., Effect of pH on magnetic properties of doped barium hexa ferrite. *Int. J. Res. Mech. Eng. Technol.,* **2013**, 3, 171-173.

[54] Suslick, K. S.; Choe, S. B.; Cichowlas, A. A.; Grinstaff, M. W., Sonochemical synthesis of amorphous iron. *Nature,* **1991**, *353*, 414-416, DOI: 10.1038/353414a0.

[55] Dimitrakopoulou, D.; Rethemiotaki, I.; Frontistis, Z.; Xekoukoulotakis, N. P.; Venieri, D.; Mantzavinos, D., Degradation, mineralization and antibiotic inactivation of amoxicillin by UV-A/TiO_2 photocatalysis. *J. Environ. Manag.,* **2012**, *98*, 168-174, DOI: 10.1016/j.jenvman.2012.01.010.

[56] Kockler, J.; Kanakaraju, D.; Glass, B.; Oelgemoller, M., Photochemical and photocatalytic degradation of diclofenac and amoxicillin using natural and simulated sunlight. *J. Sustain. Sci. Manag.,* **2012**, *7*, 23-29.

[57] Gomes da Silva, C.; Faria, J. L., Photochemical and photocatalytic degradation of an azo dye in aqueous solution by UV irradiation. *J. Photochem. Photobiol. A: Chem.,* **2003**, *155*, 133-143, DOI: 10.1016/S1010-6030(02)00374-X.